Available online at www.sciencedirect.com

SciVerse ScienceDirect

Ceramics International 39 (2013) S139–S143

CERAMICS INTERNATIONAL

www.elsevier.com/locate/ceramint

# The effect of morphotropic phase boundary on dielectric properties of $Bi_{0.5}Na_{0.5}Ti_{1-x}Zr_xO_3$ solid solutions

Ampika Rachakom[a], Sukanda Jiansirisomboon[a,b], Anucha Watcharapasorn[a,b,*]

[a]Department of Physics and Materials Science, Faculty of Science, Chiang Mai University, Chiang Mai 50200, Thailand
[b]Materials Science Research Center, Faculty of Science, Chiang Mai University, Chiang Mai 50200, Thailand

Available online 26 October 2012

**Abstract**

Lead-free bismuth sodium titanate zirconate ($Bi_{0.5}Na_{0.5}Ti_{1-x}Zr_xO_3$ or BNTZ) solid solutions with varied composition of $x=0.50$, 0.55, 0.58, 0.60, 0.63, 0.65, 0.68, 0.70, 0.73, 0.75 and 0.78 mol fraction were obtained using a conventional mixed-oxide method. XRD analysis indicated that the increase in concentration of Zr led to compositions across morphotropic phase boundary region. A quantitative structural investigation was carried out using the X-ray powder diffraction data. The rhombohedral phase was found to dominate for $x<0.68$ with space group *R*3*c*. In the morphotropic phase boundary (MPB) region i.e. $0.68\leq x\leq 0.75$, it was demonstrated that coexistence of rhombohedral and orthorhombic phase was observed. For $x=0.78$, the phase was completely orthorhombic with space group *Pmna*. Furthermore, the dielectric properties showed some enhanced activity of dipole movement at MPB boundaries which supported the presence of MPB region in this material system.


*Keywords:* B. X-ray method; C. Dielectric properties; Bismuth sodium titanate

## 1. Introduction

Lead-based $Pb(Zr_xTi_{1-x})O_3$ system is considered to possess outstanding dielectric and piezoelectric properties which are appropriate for many applications such as capacitor, sensor, actuator and other piezoelectric devices. These solid solutions consist of isovalent substitution of $Zr^{4+}$ for $Ti^{4+}$sites in $PbTiO_3$. The results of this substitution include distortion of crystal structure and composition-induced phase transition for atomic ratio of Zr/Ti around 52/48 which separates the Zr-rich phase rhombohedral region (space group *R*3*c* and *R*3*m*) from Ti-rich tetragonal region (space group *P*4*mn*), so-called morphotropic phase boundary (MPB). This region incorporated co-existing tetragonal and rhombohedral ferroelectric domains, leading to enhanced polarizability and was therefore exploited as a potential piezoelectric material [1–3]. Subsequently, there have been numerous reports on the structural investigation carried out on PZT system. Many PZT-related researches have led to further studies of structure and phase for other MPB systems such as lead-based PMN–PT [4], PZN–PT [5] and lead-free BNT–BKT–BT [6]. However, current environmental, health, and social aspects have demanded to reduce and ultimately eliminate the Pb-content of this type of materials. $Bi_{0.5}Na_{0.5}TiO_3$ is one candidate of lead-free piezoelectric ceramics due to its strong ferroelectric behavior at room temperature [7,8]. Consequently, the structure and phase transition of BNT single crystal were studied by using neutron diffraction. The refinements have revealed the sequence of phase transition from high temperature cubic structure, to one of tetragonal and then rhombohedral phase at room temperature [9]. Hence, the purpose of the present study is to investigate morphotropic phase boundary of $Bi_{0.5}Na_{0.5}Ti_{1-x}Zr_xO_3$ system (where $x=0.50$, 0.55, 0.58, 0.60, 0.63, 0.65, 0.68, 0.70, 0.73, 0.75 and 0.78 mol fraction) and carries out quantitative phase analysis based on the X-ray diffraction data. In addition, the relationships between crystal structure, physical and dielectric properties are obtained and discussed.

*Corresponding author at: Department of Physics and Materials Science, Faculty of Science, Chiang Mai University, Chiang Mai 50200, Thailand.
*E-mail address:* anucha@stanfordalumni.org (A. Watcharapasorn).

0272-8842/$ - see front matter © 2012 Elsevier Ltd and Techna Group S.r.l. All rights reserved.
http://dx.doi.org/10.1016/j.ceramint.2012.10.050

## 2. Experimental procedure

$Bi_{0.5}Na_{0.5}Ti_{1-x}Zr_xO_3$ or BNTZ ceramics with $x=0.50$, 0.55, 0.58, 0.60, 0.63, 0.65, 0.68, 0.70, 0.73, 0.75 and 0.78 mol fraction were prepared by the solid state reaction method. The starting materials for preparing ceramics included stoichiometric amount of reagent powders of $Bi_2O_3$ (>98%, Fluka), $Na_2CO_3$ (99.5%, Carlo Erba), $TiO_2$ (>99%, Riedel de Haël]n) and $ZrO_2$ (>99%, Riedel de Haël]n) which were mixed in ethanol using zirconia ball milling media for 24 h. The milled powders were dried prior to the calcination step which was carried out at 800 °C/2 h and then ball milled again for 6 h. Phase development and crystallographic structure of the powders were examined by the X-ray diffraction (XRD, Rikagu mini flex II) with $CuK_\alpha$ radiation. The calcined powders were uniaxially pressed into pellets at a pressure of 5.5 MPa with a few drops of 3 wt% polyvinyl alcohol (PVA) used as a binder before being sintered at 950 °C for 2 h and re-checked for phase purity using the X-ray diffractometer. The preliminary crystal structure details were calculated using the Powder Cell program [10], with fitting parameters based on the X-ray diffraction pattern of BNTZ powder. The peak shape was modeled as a pseudo-Voigt function, taking into account both Gaussian and Lorentzian broadening. The density and microstructure of ceramics were evaluated by the Archimedes method and the scanning electron microscopy (SEM, JEOL JSM-6335F), respectively. The grain size was determined from the SEM micrograph using the mean linear interception method. Dielectric constant ($\varepsilon_r$) and loss tangent ($\tan\delta$) were measured at room temperature with frequency in between 1 and 1000 kHz using the LCZ meter (LF Impedance Analyzer 4292A).

## 3. Results and discussion

X-ray diffraction patterns of synthesized $Bi_{0.5}Na_{0.5}Ti_{1-x}Zr_xO_3$ solid solutions are demonstrated in Fig. 1(a). All patterns showed homogeneous phase except small amount of Zr-rich phase (i.e. peak at $2\theta\sim28°$) for sample with $x>0.65$ mol fraction. Generally, all peaks were found to systematically shift toward lower angles as Zr concentration increased. This was apparently associated with the difference in size of ionic radii of $Zr^{4+}$ (~0.71 Å) when it substituted into $Ti^{4+}$ (~0.64 Å) [11]. The variation in peak shape and position of $Bi_{0.5}Na_{0.5}Ti_{1-x}Zr_xO_3$ system was analyzed and shown in Fig. 1(b) in order to locate the MPB region in this system. Initial calculated patterns were assigned to rhombohedral phase with space group *R*3*c* which has a polar symmetry permitting ferroelectricity [10] and orthorhombic phase with space group *Pmna* based on the most probable general space group for Zr-rich solid solutions which were reported to have antiferroelectric behavior at ambient temperature [12]. Considering the overlap of observed and calculated peaks as plotted in solid black and red lines, respectively, the fitting results implied that the compositions $x=0.50$–0.65 showed peak characteristics for rhombohedral symmetry while the composition $x=0.78$ showed peak characteristics for orthorhombic symmetry and both structures coexisted between $x=0.68$ and 0.75 mol fraction.

The effect of BNTZ composition on position and intensity of selected XRD reflection peaks are shown in

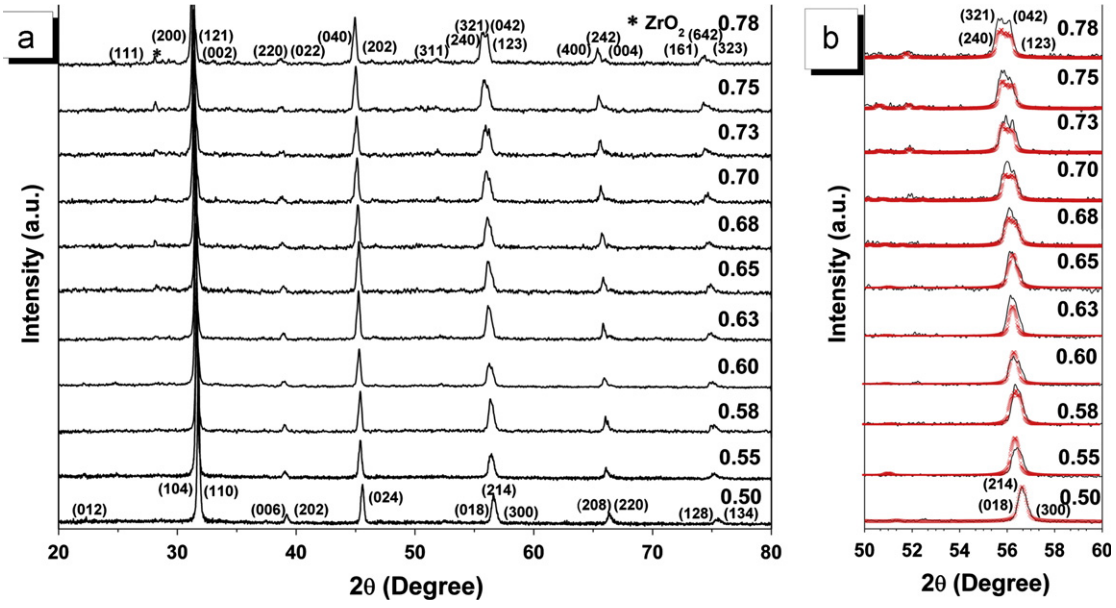


Fig. 1. (a) XRD patterns of the $Bi_{0.5}Na_{0.5}Ti_{1-x}Zr_xO_3$ powders and (b) the variations in the X-ray peaks of $Bi_{0.5}Na_{0.5}Ti_{1-x}Zr_xO_3$ powders compared betweens observed (black line) and calculated (red line) pattern in the $2\theta$ range of 50–60°. (For interpretation of the references to color in this figure legend, the reader is referred to the web version of this article.)

Table 1
The physical properties, crystal structure details and quantitative phase analysis of $Bi_{0.5}Na_{0.5}Ti_{1-x}Zr_xO_3$ system.

| $x$ | Physical properties | | Lattice parameter (Å) | | | $\alpha$ (°) | $V$ (Å$^3$) | Quantitative phase analysis (vol%) | |
|---|---|---|---|---|---|---|---|---|---|
| | Density (g/cm$^3$) | Average grain size (μm) | $a$ | $b$ | $c$ | | | $R$ | $O$ |
| 0.50 | 5.27 ± 0.016 | 5.22 ± 0.014 | | 3.975 | | 89.88 | 62.83 | 100 | – |
| 0.55 | 5.08 ± 0.050 | 5.75 ± 0.015 | | 3.976 | | 89.89 | 62.86 | 100 | – |
| 0.58 | 5.35 ± 0.021 | 5.24 ± 0.010 | | 3.987 | | 89.77 | 62.62 | 100 | – |
| 0.60 | 5.36 ± 0.014 | 7.69 ± 0.016 | | 3.987 | | 89.82 | 62.54 | 100 | – |
| 0.63 | 5.01 ± 0.023 | 5.91 ± 0.015 | | 3.996 | | 89.98 | 63.80 | 100 | – |
| 0.65 | 5.20 ± 0.011 | 6.65 ± 0.026 | | 3.990 | | 89.86 | 63.53 | 100 | – |
| 0.68 | 5.37 ± 0.027 | 6.38 ± 0.015 | | 4.007 | | 90.08 | 64.35 | 89.1 | 10.9 |
| | | | 5.6250 | 8.0245 | 5.6921 | 90.00 | 256.92 | | |
| 0.70 | 5.14 ± 0.039 | 6.28 ± 0.015 | | 4.029 | | 90.13 | 65.40 | 72.8 | 27.2 |
| | | | 5.6218 | 7.9954 | 5.7576 | 90.00 | 258.79 | | |
| 0.73 | 5.24 ± 0.036 | 6.51 ± 0.018 | | 4.026 | | 89.80 | 65.26 | 68.5 | 31.5 |
| | | | 5.6995 | 8.0500 | 5.6269 | 90.00 | 258.16 | | |
| 0.75 | 5.420 ± 0.043 | 4.92 ± 0.011 | | 4.025 | | 89.95 | 65.23 | 41.2 | 58.8 |
| | | | 5.6678 | 8.0122 | 5.6618 | 90.00 | 257.11 | | |
| 0.78 | 5.283 ± 0.032 | 6.78 ± 0.018 | 5.7212 | 8.0883 | 5.6664 | 90.00 | 262.21 | – | 100 |

Fig. 2. The crystal structure details from quantitative analysis of these peaks were also tabulated in Table 1. In this case, XRD peaks in the $2\theta$ range of 50–60° containing triplet lines i.e. (018), (214) and (300) reflections were used for investigating the coexistence region. Note that the blue lines indicated calculated rhombohedral and orthorhombic phases which were merged into integrated red area. Starting at $x=0.50$ mol fraction, the sharp peak of (018), (214) and (300) indicated a completely rhombohedral phase. These peaks began to broaden with increasing Zr concentration up to $x=0.65$ but still showed rhombohedral structure. At $x=0.68$, the XRD peak began to split and the peak-fitting analysis indicated a certain degree of coexistence of two structures i.e. orthorhombic and rhombohedral in an approximate volume percent ratio of 10.9:89.1 (Fig. 2b). At Zr content of $x=0.73$ and 0.75, the amount of orthorhombic phase was found to increase while rhombohedral phase decreased with corresponding volume percent ratio of 68.5:31.5 and 58.8:41.2, respectively. Finally, at $x=0.78$, a completely orthorhombic splitting of the (240), (321), (042) and (123) reflection peaks was observed. The unit-cell parameter for each composition was determined by fitting the XRD patterns of $Bi_{0.5}Na_{0.5}Ti_{1-x}Zr_xO_3$ powder as shown in Fig. 2(b). The rhombodedral $R3c$ space group was calculated from pre-assumed lattice parameter and it was used for fitting the XRD data of the samples with $x=0.50$–0.75 mol fraction whereas the orthorhombic $Pmna$ space group was used for fitting those with composition $x=0.68$–0.78 mol fraction. Based on peak-fitting analysis in the region of $0.68 < x < 0.75$, using rhombohedral or orthorhombic structure alone could not give a satisfactory result. Therefore, the parameters of $R3c$ and $Pmna$ space groups were simultaneously used for the fitting until the calculated patterns had the residual error less than 10% when compared to the observed pattern. Based on this analysis, it showed that a morphotropic phase boundary (MPB) region existed in BNTZ system and elongated rhombohedral unit cell in a face diagonal likely caused a distortion in the rhombohedral cell volume and transformed into orthorhombic structure along the axis enclosing the shear angle [1].

Backscattered electron micrographs (Fig. 3) revealed that the ceramics were homogeneous phase and could be densely sintered at 950 °C for 2 h. The general morphologies of BNTZ ceramics contained large irregular-shape grains and sporadically distributed small grains. Compositional analysis did not show any significant difference between these grains. It was likely that small grains would disappear if longer sintering time was used. The measured density of all ceramics was found to be in the range of 5.01–5.42 g/cm$^3$ which corresponded to the relative density of at least 95% of their theoretical values in agreement with the observed microstructure [13].

Fig. 4 shows dielectric constant ($\varepsilon_r$) and dielectric loss ($\tan\delta$) at 10, 20 and 100 kHz as a function of Zr-concentration in $Bi_{0.5}Na_{0.5}Ti_{1-x}Zr_xO_3$ ceramics. The two regions just outside MPB showed a slight decrease of $\varepsilon_r$ with increasing Zr concentration. Within MPB, no significant change in $\varepsilon_r$ was observed. Nevertheless, it could be seen that at the two boundaries of MPB regions, there was some enhancement of dipole and ionic movement facilitated by changes in crystal structure. Thus, this information helped to confirm the presence of MPB region in the BNTZ system.

## 4. Conclusions

The present work investigated the fabrication, crystal structure details, phase transformation and dielectric properties of lead-free $Bi_{0.5}Na_{0.5}Ti_{1-x}Zr_xO_3$ (where $x=0.50$, 0.55, 0.58, 0.60, 0.63, 0.6, 0.68, 0.70, 0.73, 0.75 and 0.78 mol fraction) solid solutions. Quantitative phase analysis showed that a morphotropic phase boundary existed in the BNTZ samples with Zr content from 0.68 to 0.75 mol fraction. Dielectric properties enhancement at the two boundaries also indicated the influence of phase transition

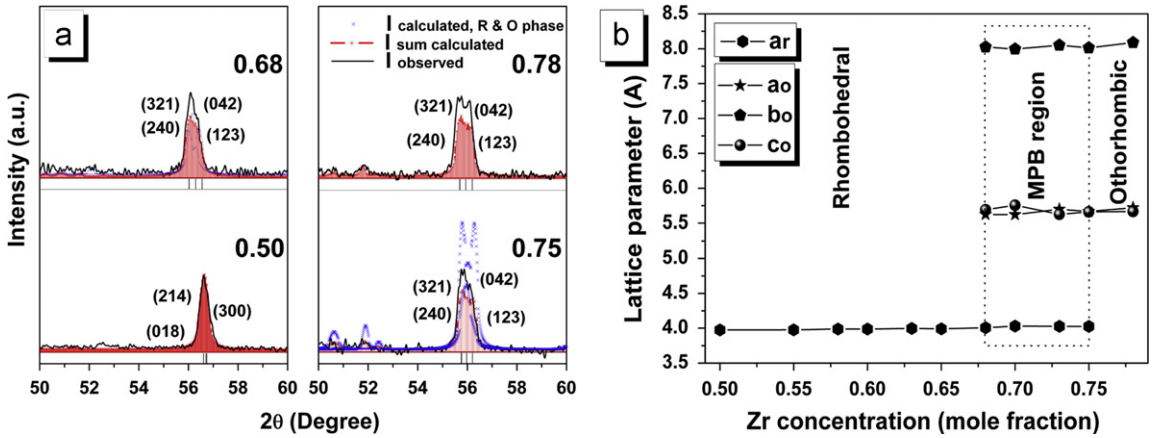


Fig. 2. (a) Sampled quantitative X-ray peak analysis of $Bi_{0.5}Na_{0.5}Ti_{1-x}Zr_xO_3$ powders with $x=0.50$, 0.68, 0.75 and 0.78 mol fraction and (b) lattice parameter of $Bi_{0.5}Na_{0.5}Ti_{1-x}Zr_xO_3$ system. (For interpretation of the references to color in this figure, the reader is referred to the web version of this article.)

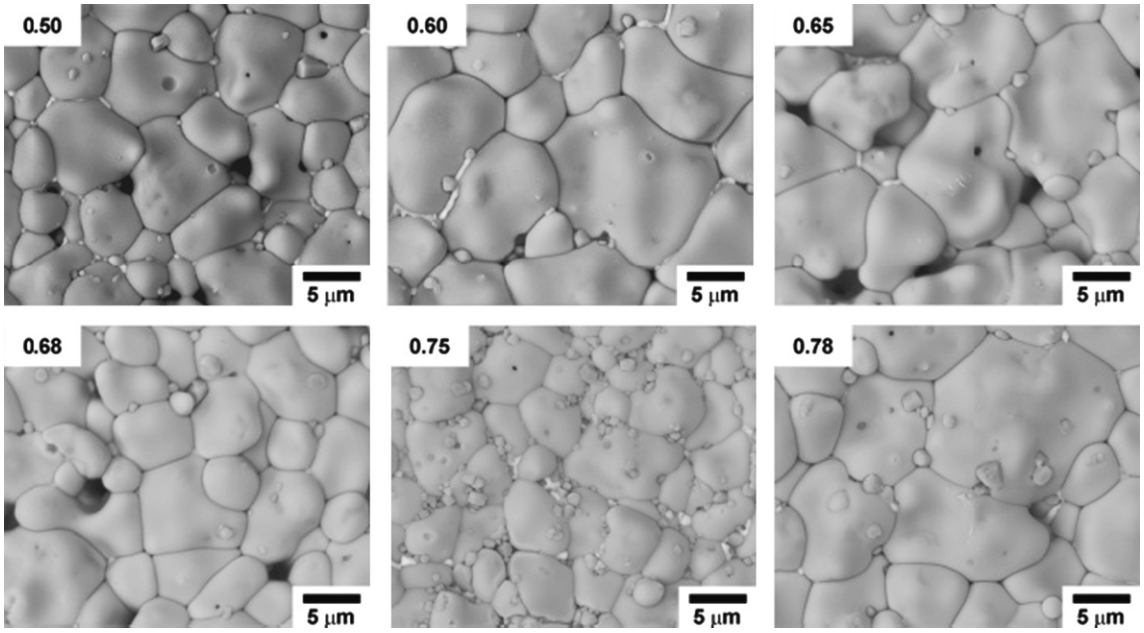


Fig. 3. Backscattered electron images of as sintered $Bi_{0.5}Na_{0.5}Ti_{1-x}Zr_xO_3$ ceramics with $x=0.50$, 0.60, 0.65, 0.68, 0.75 and 0.78 mole fraction.

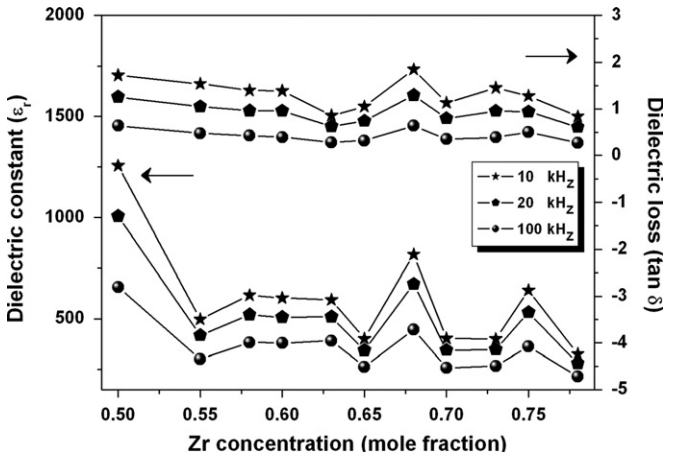


Fig. 4. Dielectric constant ($\varepsilon_r$) and dielectric loss ($\tan\delta$) at 10, 20 and 100 kHz of $Bi_{0.5}Na_{0.5}Ti_{1-x}Zr_xO_3$ ceramics.

in this material system. Further analysis on properties of BNTZ ceramics at MPB would provide useful information for possible applications of these compounds.

## Acknowledgments

This work was financially supported by the National Metal and Materials Technology Center (MTEC), the Nation Science and Technology Development Agency (NSTDA), the Thailand Research Fund (TRF) and the National Research University Project under Thailand's Office of the Higher Education Commission (OHEC). The Faculty of Science and the Graduate School, Chiang Mai University is also acknowledged. Ms. Ampika Rachakom would like to thank the Commission on Higher Education for supporting by grant fund under the program Strategic

Scholarships for Frontier Research Network for the Ph.D. Program Thai Doctoral degree for this research.

## References

[1] B. Jaffe, W.R. Cook, H. Jaffe, Piezoelectric Ceramics, Academic Press, London, UK, 1971.
[2] G.H. Haertling, Ferroelectric ceramics: history and technology, Journal of the American Ceramic Society 82 (4) (1999) 797–818.
[3] A.J. Moulson, J.M. Herbert, Electroceramics: Materials, Properties, Applications, John Wiley & Sons, Chichester, 2003.
[4] Y. Guo, H. Luo, D. Ling, H. Xu, T. He, Z. Yin, The phase transition sequence and the location of the morphotropic phase boundary region in $(1-x)[Pb(Mg_{1/3}Nb_{2/3})O_3]_{1-x}PbTiO_3$ single crystal, Journal of Physics: Condensed Matter 15 (2003) L77–L82.
[5] Z.G. Ye, B. Noheda, M. Dong, D.E. Cox, G. Shirane, Monoclinic phase in the relaxor-based piezoelectric ferroelectric $Pb(Mg_{1/3}Nb_{2/3})O_3$–$PbTiO_3$ system, Physical Review B 64 (2001) 184114.
[6] J.-F. Trelcat, C. Courtois, M. Rguiti, A. Leriche, P.-H. Duvigneaud, T. Segato, Morphotropic phase boundary in the BNT–BT–BKT system, Ceramics International 38 (2011) 2823–2827.
[7] G.A. Smolenskii, V.A. Isupov, A.I. Angranovskaya, N.N. Krainik, New ferroelectric of complex composition, Soviet Physics-Solid State (English Translation) 2 (1961) 2651–2654.
[8] T. Takenaka, K. Sakata, K. Toda, Piezoelectric properties of $(Bi_{1/2}Na_{1/2})TiO_3$-based ceramics, Ferroelectrics 169 (1995) 317–325.
[9] G.O. Jones, P.A. Thomas, Investigation of the structure and phase transition in the novel A-site substituted distorted perovskite compound $Na_{0.5}Bi_{0.5}TiO_3$, Acta Crystallographica Section B: Structural Science B58 (2002) 168–178.
[10] W. Kraus, G. Nolze, A program for the representation and manipulation of crystal structures and calculation of the resulting X-ray powder patterns, Journal of Applied Crystallography 29 (1996) 301–303.
[11] R.D. Shannon, Revised effective ionic radii and systematic studies of interatomic distances in halides and chalogenides, Acta Crystallographica Section A A32 (1976) 751–767.
[12] K. Lily, K. Kumari, K. Prasad, K.L. Yadav, Dielectric and impedance study of lead-free ceramics $(Na_{0.5}Bi_{0.5})ZrO_3$, Journal of Materials Science 42 (2007) 6252–6259.
[13] P. Jaiban, A. Rachakom, S. Buntham, S. Jiansirisomboon, A. Watcharapasorn, Fabrication of $Bi_{0.5}Na_{0.5}ZrO_3$ powder by mixed oxide method, Materials Science Forum 695 (2001) 49–52.